AD-A069 563 JOINT INST FOR LAB ASTROPHYSICS BOULDER COLO F/G 7/4
PHOTODETACHMENT STUDIES OF MOLECULAR NEGATIVE IONS.(U)
APR 79 W C LINEBERGER DAAG29-76-G-0236

UNCLASSIFIED ARO-14118.1-P NL

| OF |
AD A069563

END
DATE FILMED
7-79
DDC

ARO 14118.1-P and 16023.1-P

(12)

LEVEL II

PHOTODETACHMENT STUDIES OF MOLECULAR NEGATIVE IONS

A031059

Final Report

W. C. Lineberger

1 April 1979

U. S. ARMY RESEARCH OFFICE

76-G-0236;

Grant Number DAAG29-78-G-0096

Joint Institute for Laboratory Astrophysics
University of Colorado
Boulder, Colorado 80309

Approved for Public Release;
Distribution Unlimited

Unclassified

SECURITY CLASSIFICATION OF THIS PAGE (When Data Entered)

REPORT DOCUMENTATION PAGE

READ INSTRUCTIONS BEFORE COMPLETING FORM

1. REPORT NUMBER: FINAL REPORT
2. GOVT ACCESSION NO.
3. RECIPIENT'S CATALOG NUMBER
4. TITLE (and Subtitle): Photodetachment Studies of Molecular Negative Ions,
5. TYPE OF REPORT & PERIOD COVERED: Final Report, 15 APR 76-31 DEC 78
6. PERFORMING ORG. REPORT NUMBER
7. AUTHOR(s): W. C. Lineberger
8. CONTRACT OR GRANT NUMBER(s): DAAG29-76-G-0236, DAAG29-78-G-0096
9. PERFORMING ORGANIZATION NAME AND ADDRESS: Joint Institute for Laboratory Astrophysics, University of Colorado, Boulder, Colorado 80309
10. PROGRAM ELEMENT, PROJECT, TASK AREA & WORK UNIT NUMBERS
11. CONTROLLING OFFICE NAME AND ADDRESS: U. S. Army Research Office, P. O. Box 12211, Research Triangle Park, NC 27709
12. REPORT DATE: 1 April 1979
13. NUMBER OF PAGES: 46p.
14. MONITORING AGENCY NAME & ADDRESS (if different from Controlling Office)
15. SECURITY CLASS. (of this report): Unclassified
15a. DECLASSIFICATION/DOWNGRADING SCHEDULE
16. DISTRIBUTION STATEMENT (of this Report): Approved for public release; distribution unlimited.
17. DISTRIBUTION STATEMENT (of the abstract entered in Block 20, if different from Report)
18. SUPPLEMENTARY NOTES: The view, opinions, and/or findings contained in this report are those of the author(s) and should not be construed as an official Department of the Army position, policy, or decision, unless so designated by other documentation.
19. KEY WORDS (Continue on reverse side if necessary and identify by block number): Molecular Negative Ions, Photodetachment, O_3^-
20. ABSTRACT (Continue on reverse side if necessary and identify by block number)

Photoelectron spectrometry and threshold photodetachment spectroscopy have been used to obtain the electron affinity of O_3^- (2.1028 eV). A photodissociation model is proposed.

DD FORM 1 JAN 73 1473 EDITION OF 1 NOV 65 IS OBSOLETE

192 900

Unclassified

SECURITY CLASSIFICATION OF THIS PAGE (When Data Entered)

PHOTODETACHMENT STUDIES OF MOLECULAR NEGATIVE IONS

During the eight-month period of this grant, we have completed studies of the photodetachment and photodissociation of O_3^-, and obtained the electron affinity of O_3, 2.1028 eV. The threshold photodetachment region is characterized by a striking competition between photodissociation and photodetachment. Based upon these data we propose a model for photodissociation of O_3^- which involves a symmetric transition state. A paper describing these results will be published in the Journal of Chemical Physics in March 1979; a copy of this paper is included as Appendix A.

Project personnel during this period were W. C. Lineberger and Mr. P. L. Jones, a graduate student in the Department of Chemistry at the University of Colorado.

APPENDIX A

Laser photoelectron, photodetachment, and photodestruction spectra of O_3^-

Stewart E. Novick*, Paul C. Engelking†, Patrick L. Jones, Jean H. Futrell‡ and W. C. Lineberger§

Department of Chemistry, University of Colorado and
Joint Institute for Laboratory Astrophysics
University of Colorado and National Bureau of Standards
Boulder, Colorado 80309

(Received 29 August 1978)

Abstract

Fixed frequency laser photoelectron spectrometry and variable frequency laser photodetachment and photodestruction spectroscopy of the ozonide ion, O_3^-, have been accomplished. The electron affinity of ozone is measured to be $EA(O_3) = 2.1028(25)$ eV, in good agreement with previous measurements of less accuracy. Progressions in the spectra are analyzed to yield the symmetric stretching frequency and the bending frequency of the ozonide ion to be 982(30) cm^{-1} and 550(50) cm^{-1} respectively. While no evidence is found for a long lived excited electronic state of O_3^-, an excited electronic state of neutral ozone is found roughly 0.7 - 1.1 eV above the ground state. Models for the dissociation of O_3^- are examined to explain why the photoelectron and photodetachment spectra fail to show a strong progression in the symmetric bending vibrational mode. Attempts to measure the electron affinity of CO_3^- were unsuccessful. Limits placed by this attempt and our $EA(O_3)$ value are invoked in a discussion of some recent disagreements in the literature on the thermochemistry of CO_3^- and O_3^-.

I. INTRODUCTION

Ozone and its negative ion play an important role in the chemistry of the upper atmosphere.[1] Consequently there has been a large investment of experimental effort in the study of the thermochemistry and spectroscopy of O_3 and O_3^-. The kinetic measurements include the study of the reaction $O_3^- + CO_2 \rightarrow CO_3^- + O_2$ using a variable-temperature flowing afterglow apparatus,[2] mass spectrometric studies of the reactions of neutral ozone with a series of negative ions[3] and threshold measurements for collision-induced dissociation of O_3^- upon impact with various target gases.[4] The spectroscopic studies include measurement of the photodissociation cross section[5-7] ($O_3^- + h\nu \rightarrow O_2 + O^-$), observations of excited states in neutral ozone near the dissociation limit using electron energy loss spectroscopy,[8] and measurement of the photodetachment of O_3^- ($O_3^- + h\nu \rightarrow O_3 + e^-$) using drift tube techniques and a series of colored filters.[9,10]

The present study consists of two independent crossed ion beam-laser beam photodetachment experiments on O_3^-. In the first experiment (laser photoelectron spectrometry) a fixed frequency Ar^+ laser beam is crossed with a mass selected beam of O_3^- and the resulting photodetached electrons are energy analyzed with a resolution of approximately 60 meV (480 cm^{-1}). In the second experiment (tunable laser photodetachment) the beam from a tunable cw jet stream dye laser with a resolution of between 1-10 cm^{-1} (0.1 - 1.2 meV) is crossed with the mass selected O_3^- ion beam. Two different neutral particles can be produced, O_3 resulting from photodetachment, and O_2 resulting from photodissociation. Both O_3 and O_2 are detected together, providing a measurement of total photodestruction cross section, as a function of laser frequency. The photodetached electrons are also counted (but not energy analyzed) as a function of the frequency of the laser, resulting in a measurement of the threshold photodetachment cross section.

Our initial motivation for the study of the photodetachment of O_3^- was to provide an accurate value for the electron affinity of ozone. This was deemed necessary because of the significant differences among the thermochemical data generated by some of the kinetic and spectroscopic studies. The value of the electron affinity of ozone has been used to complete thermochemical cycles to deduce, for example, the dissociation energy of O_3^-, $D_0(O_2\text{-}O^-)$ values of which vary between an upper limit of 1.3 eV and lower limit of 1.6 eV.[2,5] The collision induced dissociation experiments[4] determine this energy to be 1.8 ± 0.1 eV. Prior to this study, the most definitive determination of the electron affinity of ozone was given by the onset of O_3^- photodetachment in a drift tube with a broadband light source, resulting[9] in $EA(O_3)$ = 1.99 ± 0.1 eV.

II. EXPERIMENTAL

A. Laser photoelectron spectrometry

The fixed frequency photodetachment apparatus has been described previously.[11] Ozone, evolving from a cooled (-77°C) silica gel surface, is burned in a low pressure (1 Torr) electrical discharge ion source to produce beams of O_3^- $O_3 + e^- \rightarrow O^- + O_2$ followed by $O^- + O_3 \rightarrow O_3^- + O$ is the likely ion production scheme. The ions are extracted from the source, accelerated to 680 eV, and mass analyzed by an $\underline{E}\times\underline{B}$ (Wien) filter. Beams of O_3^- of 10-100 nA are crossed in a field free interaction region by the intracavity beam of a cw Ar^+ laser, and the electrons ejected into the acceptance angle of a hemispherical electrostatic energy selector are energy analyzed with a resolution of 60 meV FWHM. At this resolution the many rotational components of a single vibronic transition are smoothed to a nearly Gaussian peak shape. The Ar^+ laser is operated on a single line (with the ion beam inside the laser cavity) at either 4880 Å (2.540 eV) or in the UV at 3638 Å (3.407 eV). A reflective beam expander is used intracavity to match the laser beam to the ion beam. Single line operation in the visible is achieved with the usual Littrow prism. Wavelength selective reflective coatings are used for single line uv operation. The single line performance is checked with a spectrometer and by insuring that the photoelectron spectrum of O^- consists of a single peak. Circulating powers are ~200 W in the visible and ~10 W in the ultraviolet.

The spectra are "self calibrated" in that along with photodetachment, photodissociation occurs; $O_3^- + h\nu \rightarrow O_2 + O^-$ followed by photodetachment of the oxide ion, $O^- + h\nu \rightarrow O + e^-$, results in a substantial O^- photodetachment signal when O_3^- is irradiated. The effective (weighted average of the fine structure components) electron affinity of atomic oxygen is known precisely,

E.A.(O) = 1.465 eV.[12] The absolute detachment energies of peaks in the spectra are determined by E_x = E.A.(O) + 1.044($\Omega_{O^-} - \Omega_{X^-}$) where ($\Omega_{O^-} - \Omega_{X^-}$) is the laboratory energy difference between the O^- peak center and a particular X^- peak center. The factor 1.044 is an energy scale compression factor calculated by calibrating an O_2^- photodetachment spectrum (also conveniently produced by the burning of ozone under identical source conditions) against the known O_2 $^3\Sigma(v=1)$, $^1\Delta(v=1)$ splitting.[13] The usual kinetic shift correction term[11] is not present in the above expression because the velocity of O_3^- and of the O^- resulting from photodissociation are essentially identical. In both this apparatus and the tunable laser apparatus, approximately 30 μsec elapse between ion formation and interaction with the laser beam.

B. Tunable laser photodetachment

The tunable laser photodetachment apparatus has also been described elsewhere.[14] This apparatus is capable of simultaneous detection of both the electrons and the neutral products of photodetachment and photodissociation.

O_3^- is produced as in part A and mass selected through a 90° sector magnet. Beams of O_3^- of approximately 10 nA and an energy of 1000 eV are crossed with the intracavity radiation of an Ar^+ pumped cw jet stream dye laser using either Rhodamine 6G or Rhodamine 110 as the lasing medium. The dye laser is used intracavity by replacing the 3% transmitting flat output mirror with a >99.5% reflective one meter radius of curvature back mirror to extend the length of the laser cavity by one meter. The ion and laser beams cross at 90° in an interaction region which consists of cylindrical block machined from a single piece of molybdenum (to avoid spurious electric fields) with appropriate aperture holes for the beams and for the draw out of photodetached electrons. While complete energy analysis of the detached electrons is not attempted, it is possible and advantageous to discriminate between fast and slow (<100 meV) electrons.

By choosing to observe only slow electrons, threshold features in the photodetachment cross section can be observed with an enhanced signal-to-noise ratio. Such features result from the opening of a new channel, generating slow electrons at or near threshold for that channel. By observing primarily the slow electrons, these thresholds can be observed without being swamped by the fast electrons from the sum of all the previously opened channels. This selection is accomplished by supplying a very weak extraction field (~1 V/m) which will extract slow electrons from the interaction region while fast electrons are largely unaffected by the field and primarily strike the walls of the interaction region where they are absorbed by the gold-blacked surface of the molybdenum cylinder.

Along with photodetachment, photodissociation of O_3^- to produce molecular oxygen and the atomic negative ion may occur. All the heavy particles, the negative ions O_3^- and O^- and the neutrals O_3 and O_2, travel through the interaction region to a heavy-particle separator which consists of various electrostatic deflection plates as described in Ref. 14a. The undeflected neutral molecules (with typical kinetic energy of 700-1000 eV) are detected by secondary electron emission using a continuous-dynode electron multiplier. The neutral detection scheme thus does not differentiate between photodetachment and photodissociation but measures their sum, the photodestruction cross section. The negative ion flux, completely dominated by unaffected O_3^-, is deflected by the heavy-particle separator into a Faraday cup.

The electron channeltron, the neutral molecule electron multiplier, and the negative ion Faraday cup are all interfaced to a PDP-8E computer. The computer also monitors the laser flux, controls the tunable laser frequency, and makes appropriate background corrections to the detected signal levels.

III. RESULTS

A. Laser photoelectron spectra

Figure 1 shows the O_3^- photoelectron spectrum obtained with ~200 circulating watts of 2.540 eV photons, and Fig. 2 that obtained with ~10 circulating watts of 3.407 eV photons. The spacing of the main progressions in the figures are indicative of the ν_1 symmetric stretch in the neutral and negative ion. In the figures we use the notation 1_a^b to represent $O_3^-(v_1 = a, 0, 0) \rightarrow O_3(v_1 = b, 0, 0)$ and 2_a^b to represent $O_3^-(0, v_2 = a, 0) \rightarrow O_3(0, v_2 = b, 0)$. By fitting Gaussian peak shapes to the observed spectra we find the splitting between the peaks labeled 1_0^1 and 0-0 is 1090(30) cm^{-1} and the splitting between the peaks 0-0 and 1_1^0 is 1040(60) cm^{-1}. Since the ν_1 symmetric stretching frequency in neutral ozone is known to be 1103 cm^{-1} from infrared spectra[15,16] we can make the tentative identification that the peak labeled 0-0 is in fact the

$$O_3^-(v_1=0,v_2=0,v_3=0) \rightarrow O_3(v_1=0,v_2=0,v_3=0)$$

transition. This identification and the electron kinetic energy at peak center give the electron affinity of ozone to be 2.124(30) eV uncorrected for rotational effects; upon incorporation of rotational corrections, we obtain $EA(O_3)$ = 2.103(20) eV (see next section; there we also give a more precise value of the electron affinity deduced from the tunable laser experiments). The progression on the low electron energy side of the 0-0 peak is identified as the progression in ν_1 of O_3, and the peaks to the high electron energy side of the 0-0 peak are the progression and their associated sequence bands in the symmetric stretch of O_3^- (hot bands) with a frequency $\nu_1(O_3^-)$ = 1040(60) cm^{-1}. Matrix[17] and crystal[18,19] studies place this number between 1012 and 1032 cm^{-1}.

While the gas discharge ion source produces ions in an unknown distribution of initial vibrational states, peaks in the photoelectron spectra can frequently be recognized as arising from hot bands if they vary relative to other peaks as ion source operating conditions are charged. This procedure is only qualitative; the most effective step is to vary the ion vibrational "temperature" by changing the potential which extracts the ions from the high pressure source into the "collision free" part of the beam machine. The assignment of the transitions labelled 1_1^0, 1_2^0, and 1_3^0 as arising from excited vibrational levels was confirmed by altering the ion beam vibrational "temperature" by large changes in this extraction voltage. It was possible to vary the beam temperature in this way from approximately 1000 to 600 K and to observe the change in the relative intensity of the hot bands with respect to the 0-0, 1_0^1, 1_0^2, 1_0^3 peaks, the progression in ν_1 of neutral ozone.

The asymmetric stretch, ν_3, transforms as the irreducible representation B_2 of group C_{2v} and as such only transitions of zero or an even number of quanta have nonzero Franck-Condon overlaps. Furthermore as long as both O_3 and O_3^- have symmetry C_{2v} the intensity for $\Delta v_3 = \pm 2, \pm 4 \ldots$ will be very small with respect to the intensity of $\Delta v_3 = 0$, even for the case where there is a sizeable displacement in the equilibrium bond lengths of the neutral and the negative ion. This is because the potential minimum occurs at the same value of the ν_3 normal coordinate (namely zero) for both the neutral and the ion (see Ref. 20, pp. 151-153). The net effect of all this is that a progression in ν_3 should not be present in the photoelectron spectra.

It should be noted that the photoelectron spectra show no evidence of a progression in ν_2, the symmetric bend. There is no group theoretic reason

for this, and indeed the photoelectron spectrum of the related negative ion SO_2^- very clearly shows a progression in both ν_1 and ν_2.[11b] The explanation for the lack of a ν_2 progression in the spectra will be sought in the dynamics of the photodetachment/photodissociation process for O_3^- in a later section.

Figure 2 shows an unassigned series of peaks at electron kinetic energy of between 0.5 and 0.8 eV. These peaks correspond to a new electronic state of neutral ozone, a state that most probably is not optically accessible from the ground state of ozone. We cannot assign the 0-0 band and so cannot make a more definite energy assignment. It appears that this state is perhaps 0.7 to 1.1 eV (6000-9000 cm^{-1}) above the ground state. (The lowest known excited electron state of ozone is 10,000 cm^{-1} above the X^1A_1 state.) Recent calculations suggest that a symmetrical state of neutral ozone (D_{3h}) might lie at or about this energy.[21-24] Triplet states also lie in this region, and might be responsible for the progression.

The last feature of the photoelectron spectra that requires explanation is the single sharp peak of Fig. 1 at an electron kinetic energy of 1.07 eV. As was briefly discussed in the experimental section this is the single peak of the photoelectron spectrum of the negative ion of atomic oxygen. The intensity of this peak is quadratic in the laser flux, indicating that two photons are required. The processes involved are photodissociation of the ozonide ion

$$O_3^- + h\nu \rightarrow O_2 + O^- \quad ,$$

followed by photodetachment of the oxide ion

$$O^- + h\nu \rightarrow O + e^- \quad .$$

Because of our lack of knowledge of the detailed geometry of the laser beam-ion beam overlap we cannot use the intensity information to extract relative photodissociation/photodetachment cross sections for O_3^-. It is clear however, that for 2.540 eV photons that the cross section for photodissociation is much larger than that for photodetachment. This result has been pointed out by other authors.[5]

The cross section for photodetachment of O^- in this photon energy range is known to be 6×10^{-18} cm^2.[25] By comparing the intensity of O^- detachment from a mass selected O^- beam (not from photodissociated O_3^-) to the integrated intensity of the O_3^- detachment signal we can deduce that the cross section for photodetachment of O_3^- with 2.540 eV photons is about 1×10^{-18} cm^2.

We also made an unsuccessful attempt to measure the electron affinity of CO_3 by photoelectron spectroscopy of CO_3^- prepared from either pure CO_2 or from a mixture of CO_2 and O_3 in the source. In the latter case no photodetached electrons could be detected, implying either that the cross section for photodetachment with 3.407 eV photons is less than 10^{-20} cm^2 or that $EA(CO_3) > 3.1$ eV (there is a low energy cutoff for electrons in our energy analyzer). While this cross section bound is smaller than might be expected, it is not inconsistent with the drift tube studies of Hong et al.[26] who reported $EA(CO_3) = 2.7$ eV. We were not able to prepare large enough beams of CO_3^- when only CO_2 was introduced into the source to attempt the measurement.

B. Tunable laser photodetachment

The lower curve of Fig. 3 shows the tunable laser photodetachment spectrum of O_3^- in the region that includes the transitions 1_1^0, 0-0, and 1_0^1 as the strong easily identifiable thresholds in the photodetachment spectrum.

As mentioned in the experimental section, the fast electrons are discriminated against, with the result that the threshold features of the spectrum are enhanced. A second consequence is that this procedure gives a somewhat distorted view of the photodetachment cross section. This distortion is by and large an artificially flattened out appearance beyond about 30 cm^{-1} above a channel opening. In reality the cross section continues to rise gently in this region until a new channel opens at which point, for a strong feature, the cross section abruptly rises in the manner shown in the figure for the transitions 0-0 and 1_0^1.

Unlike the photoelectron spectrum which has peaks corresponding to the positions of transitions between the states of the negative ion and the neutral, the photodetachment cross section shows thresholds at each new channel opening. Wigner has shown that the threshold energy dependence of the cross section is a function only of the long range forces.[27] This leads to the remarkably simple form

$$\sigma(E) \propto (E-E_0)^{(2\ell+1)/2}$$

when the only important long range force is the centrifugal barrier to detachment. Here ℓ is the angular momentum quantum number of the leaving electron and $(E-E_0)$ is the photon energy minus the transition energy (the kinetic energy of the detached electron). Brauman and coworkers have adapted[28] this result to photodetachment from polyatomic

molecules by deriving group theoretic rules for predicting the lowest allowed value of ℓ based on the irreducible representation of the highest occupied molecular orbital (HOMO) of the negative ion. Assuming that the HOMO of the negative ion is the lowest unoccupied molecular orbital of the neutral (the b_1 π^* orbital), the lowest allowed value for ℓ is determined to be 0 by Brauman's rules. Therefore the detachment partial cross section at a new rovibronic threshold is given by $\sigma \propto (E-E_0)^{1/2}$, sharp s wave detachment. For electrons detached from dipolar neutral cores the electron-dipole interaction gives rise to a long range potential of the form $\mu e \cos\theta\, r^{-2}$, where μ is the dipole moment of the neutral core, a potential of the same range as the centrifugal potential. This dipolar term can lead to the "sharpening" of the threshold law to somewhere between an $(E-E_0)^0$ and an $(E-E_0)^{1/2}$ dependence, as is apparently the case for OH^- photodetachment rotational thresholds.[29] For the present case of O_3^- detachment it is believed that the ozone dipole moment[30] of 0.5337 D is too small to affect the form of the threshold law and we assume an $(E-E_0)^{1/2}$ threshold dependence for an individual rovibronic transition.

We model a vibrational channel opening in the photodetachment spectra by assuming a cross section of the form

$$\sigma(E) \propto \sum_i (E-E_i)^{1/2}$$

where the sum is over all allowed asymmetric top rotational transitions. The electronic state of neutral ozone is of vibronic symmetry A_1 and that of the negative ion[5] is B_1; knowing this allows us to classify the individual rovibronic levels according to their irreducible representations. For C_{2v} molecules with all nuclear spins zero, rovibronic levels labeled A_1

or A_2 have a statistical weight of one while those labeled B_1 or B_2 have a statistical weight of zero.[20] In order to calculate the rotational constants of the ozonide ion we take the known averaged bond lengths and angles for the ground vibrational state of neutral ozone (r_o = 1.2792 Å, α_o = 116.77°)[31,32] and assume for the negative ion that $r_o(O_3^-) = r_o(O_3) + 0.10$ Å and $\alpha_o(O_3^-) = \alpha_o(O_3) - 3.6°$.[33] The result of the calculated modeling of the vibrational channel opening is that the sharp s-wave detachment is considerably smoothed out, in good agreement with the shapes seen in Fig. 3, and for negative ion temperatures (~1000 K) typical of our ion source the apparent channel onset is approximately 10 cm^{-1} below the true band origin. We therefore add 10 cm^{-1} to each assigned feature in the photodetachment spectra to best approximate its true origin.

Similarly, there is a rotational correction to the photoelectron spectra peak centers to obtain a best result for the band origin. The effect is larger in this case since we must unravel a peak center (high J) rather than an onset (low J). Using the same geometry estimate for O_3^- as before and a temperature of 1000°K, this rotational correction to the photoelectron shows that the origin of a peak is approximately 170 cm^{-1} to the high electron energy side of the peak center. Thus from the photoelectron spectra the electron affinity of ozone is 2.103(20) eV (16962(160) cm^{-1}). This procedure confirms our assignment of the photodetachment threshold at 16950 cm^{-1} as an origin at 16960(20) cm^{-1}, the 0-0 band origin, giving $EA(O_3)$ = 2.1028(25) eV. This is our recommended value for the electron affinity of ozone. Figure 4 shows a high resolution scan of this 0-0 transition in the photodetachment spectrum.

The lower energy threshold at 15978(20) cm^{-1} is the 1_1^0 transition, while the threshold at 18057(20) cm^{-1} is the 1_0^1 transition. We have

therefore determined from the photodetachment spectrum that $\nu_1(O_3) = 1100(30)$ cm^{-1}. The photoelectron derived value for this frequency is $\nu_1(O_3) = 1090(30)$ cm^{-1}. This number is, of course, precisely known from infrared spectra to be 1103.15 cm^{-1} [15,16]; this last result also confirms our peak identification. The symmetric stretching frequency of the negative ion from the photodetachment spectrum is 982(30) cm^{-1} which is our recommended value for this constant. The photoelectron value for this number is 1040(60) cm^{-1}. Errors in the photodetachment spectrum analysis include an inability to pick out reliably the rather gentle threshold to better than 15 cm^{-1}, and failures in the rotational modeling of the threshold. In the photoelectron spectra the major sources of error are the calibration of the electron energy analyzer and the modeling of the rotational correction.

The lower curve of Fig. 3 also shows a relatively weak sequence 0-0, 1_1^1, 1_2^2 and perhaps some higher members which we have refrained from assigning. The existence of this sequence serves as a further check on the assignment but yields essentially no new information. There should also be a sequence following 1_0^1 of Fig. 3. However the quality of the data in this green end of the spectrum is rather poor due to low laser power and we have made no attempt to assign this sequence. Table I lists all the assignments from either the photodetachment or the photodestruction data to be discussed in the next section.

The photoelectron spectra, it will be recalled, show no progression at all in ν_2, whereas harmonic oscillator Franck-Condon analysis of the ν_2 progression (and the SO_2 spectrum previously mentioned) suggest that the ν_2 progression should be almost as strong as the ν_1 progression, and clearly seen in the data. Knowing the O_3 neutral symmetric vibration frequencies from infrared data and O_3^- stretching frequency, we felt confident that

the 2_0^1 threshold would be relatively isolated and detectable ~701 cm^{-1} above the 0-0 threshold.

The photodetachment cross section of Fig. 3 shows only a very weak threshold which is assignable as that belonging to 2_0^1 -- one bending quanta of O_3 neutral following detachment. The resulting symmetric bending frequency for O_3 neutral is 720(40) cm^{-1} compared with the accurate infrared value of 700.96.[15,32] As can be seen from Fig. 3 the threshold for 2_0^1 is approximately 20 to 100 times less intense than the analogous feature in the symmetric stretch, 1_0^1, contrary to expectations.

An anomalous weakness in photodetachment transitions involving ν_2 of the negative ion also occurs. Figure 5 shows the photodetachment spectrum between the 1_1^0 and 0-0 thresholds taken at very low extraction potential (the neutral channel is independent of this parameter). Based on the observed intensity of the 1_1^0 transition (taking into account any other transitions, e.g. 1_2^1 which might contribute) the threshold from 2_1^0 should be clearly observable, but is at most barely detectable.

Raman spectra of $M^+O_3^-$ (where M = Li, Na, K, Rb, and Cs) in an argon matrix give the symmetric stretch of the ozonide ion to be 1012-1026 cm^{-1} depending on the identity of the alkali metal.[17] Single crystal Raman spectra of γ-irradiated $KClO_3$ and $NaClO_3$ show $\nu_1(O_3^-)$ to be between 1012 cm^{-1} and 1032 cm^{-1} where the spread is dependent on site effects in the crystal.[18,19] In all cases these numbers are slightly greater than our free ion value for $\nu_1(O_3^-)$. We therefore expect that $\nu_2(O_3^-)$ should be somewhat less than the matrix values of 587-619 cm^{-1} but still within approximately 100 cm^{-1} of these numbers.

Even though $\nu_2(O_3^-)$ thresholds appear to be very weak, the strongest threshold which appears in the region roughly 600 cm^{-1} below the 0-0

threshold should be 2_1^0. We thus assign the threshold in the photodetachment spectrum of Fig. 5 as that belonging to 2_1^0. The threshold has been chosen by determining the position at which the slope of the photodetachment cross section breaks. The feature assigned as 2_1^0 gives a frequency of $\nu_2(O_3^-)$ as 550(50) cm^{-1}. The vibrational information on O_3^- and O_3 is summarized in Table II.

Cosby et al.[5] have performed a tunable laser photodissociation experiment on O_3^- which shows considerable structure in the cross section for dissociation. They interpret this to mean that the O_3^- is dissociating from vibrational levels of a quasibound excited electronic state. They present two alternative assignments for the vibrational frequencies for the ground electronic state of O_3^-: I, $\nu_1(O_3^-)$ = 790(50) cm^{-1}, $\nu_2(O_3^-)$ = 419(20) cm^{-1}, and II, $\nu_1(O_3^-)$ = 930(50) cm^{-1}, $\nu_2(O_3^-)$ = 403(20) cm^{-1}. Neither of these assignments is obviously consistent with our values 982(30) cm^{-1} and 550(50) cm^{-1} for these frequencies.

C. Tunable laser photodestruction

The upper curve of Fig. 3 shows the photodestruction cross section as a function of photon frequency. The relative scales of the photodestruction and the photodetachment cross sections are obtained from the absolute counts of neutrals and electrons. The scaling is based on an approximate determination of the relative efficiency of the two detectors and is only accurate to within a factor of 3. It is clear, however, that the total photodestruction cross section is at least an order of magnitude greater than the photodetachment cross section.

The data of Fig. 3 point out one thing immediately, namely that features which show up strongly in photodetachment have at most only a minor effect on photodestruction. Thus the photodestruction cross section is a measure of the photodissociation of O_3^- into $O_2(^3\Sigma_g^-)$ and $O^-(^2P)$, the energy allowed channel. This dominance is consistent with the photodestruction measurements of Cosby et al.[5] The shape of our photodestruction cross section agrees well with that of Cosby et al.,[5] if the less thermally relaxed nature of our ions is taken into account.

Strong photodetachment thresholds make little impact upon the total photodestruction cross section. The magnitude of the total photodetachment cross section suggests that the 2_0^n ($n \geq 1$) photodetachment thresholds are anomalously weak, rather than the 1_0^n being strong. To seek an explanation of this observation we have drawn vertical lines, 2_0^1, 2_0^2, on Fig. 3 not associated with any threshold, but rather at the spectroscopically known energies above the now known 0-0 threshold. We note that at both of these locations (the only places in Fig. 3 where there are spectroscopically known 2^n thresholds) there is an apparent threshold, i.e., a change in slope, in the photodestruction cross section. This observation suggests that bending might promote dissociation when events are expected to produce O_3 $(\nu_1, \nu_2 \neq 0, \nu_3)$ + e.

IV. DISCUSSION

A. Electron affinity of ozone and its thermochemical implications

Various studies have been undertaken in the past to measure the electron affinity of ozone. These studies include photodetachment with filtered light,[9,10] collisional ionization experiments,[34] an indirect measurement by collisional bond dissociation,[4] a crystal lattice energy calculation,[35] and a C.I. level calculation of the vertical electron affinity.[36] Further, reactive thermochemical equilibrium studies carried out in a variable temperature flowing afterglow,[2] and endothermic charge transfer experiments[3,37] lead to lower limit estimates of $EA(O_3)$. These values range from 1.82 eV (a lower limit) to 2.26 eV (also a lower limit). Our value of $EA(O_3)$ = 2.1028(25) is consistent with most of the previous studies, but more accurate. These data are summarized in Table III.

We cannot clear up the thermochemical inconsistencies noted in the introduction but we can use our new value of the $EA(O_3)$ to eliminate one of the previously imprecise inputs to the cycles. As an example, we recalculate the electron affinity of CO_3^- using both the data of the flowing afterglow experiments[2] and that of the photodissociation spectroscopy of CO_3^-.[38] The electron affinity of CO_3 can be calculated with the formula

$$EA(CO_3) = +D(CO_2\text{-}O^-) - D(CO_2\text{-}O) + EA(O)$$

where the dissociation energy of CO_3 to $CO_2 + O$ is known to be 0.46(17) eV [39] and the electron affinity of oxygen is 1.462(3) eV.[12] The flowing afterglow experiments indicate that

$$D(CO_2\text{-}O^-) - D(O_2\text{-}O^-) \geq 0.58 \text{ eV} \quad .$$

Using

$$D(O_2\text{-}O^-) = EA(O_3) + D(O_2\text{-}O) - EA(O) \quad ,$$

where the dissociation of O_3 to $O_2 + O$ is known to be 1.05(2) eV,[40] we employ the flowing afterglow results to predict

$$EA(CO_3) \geq 0.58 \text{ eV} + EA(O_3) + D(O_2\text{-}O) - D(CO_2\text{-}O) \quad .$$

Thus $EA(CO_3) \geq 3.27(17)$ or rigorously 3.08 eV for a true lower limit.

The photodissociation experiments[38] measure 1.85 eV to be an upper limit to the dissociation energy of CO_3^- to $CO_2 + O^-$. The first of our thermochemical formulae gives

$$EA(CO_3) \leq 1.85 \text{ eV} - D(CO_2\text{-}O) + EA(O)$$

or $EA(CO_3) \leq 2.85(17)$ or rigorously 3.02 eV for a true upper limit. It should be noted that in both determinations of the electron affinity of CO_3 the major source of error is in the dissociation energy of neutral CO_3 and that to obtain the rigorous bounds the error of this measurement had to be subtracted in the first case and added in the second. Since there is only one true value for this dissociation the disagreement between the two determinations of $EA(CO_3)$ is the large value 0.42 eV and not the difference of the rigorous bounds. Obviously at least one of these numbers is incorrect. Collision induced dissociation studies on CO_3^- by Tiernan and coworkers[52] indicate $D(CO_2\text{-}O^-) = 2.5$ eV, and speculate that the studies of Moseley et al.[38] relate to an excited state of CO_3^-. This possibility is not confirmed by studies of the SRI group.[38]

B. The S-ructure of O_3^-

It is possible to extract structural information on O_3^- from the Franck-Condon intensity progression of the symmetric stretch displayed in Fig. 2. In the Franck-Condon approximation the vibrational band intensity is given by the square of the overlap integral,

$$F(v_1', v_2', v_3', \leftarrow v_1, v_2, v_3)$$

$$= \iiint \psi^*_{v_1'}(Q_1')\psi^*_{v_2'}(Q_2')\psi^*_{v_3'}(Q_3')\psi_{v_1}(Q_1)\psi_{v_2}(Q_2)\psi_{v_3}(Q_3)dQ_1dQ_2dQ_3$$

where the unprimed variables represent O_3^- and the primed variables represent O_3. The vibrational wavefunctions are functions of the normal coordinates Q_i where i = 1,2,3 are the symmetric stretch (A_1 under C_{2v}), symmetric bend (A_1) and asymmetric stretch (B_2). The ψ's are one dimensional harmonic oscillator functions and the integral is arbitrarily taken over the O_3^- coordinates. Duschinsky[41] first showed that the Q' can be expressed in terms of the Q by the expression

$$\underline{Q}' = \underline{\underline{J}}\,\underline{Q} + \underline{K}$$

where $\underline{\underline{J}}$ is (usually) an orthogonal matrix and is block diagonalized by irreducible representations and the $\underline{K}$ vector has non-zero elements only for totally symmetric modes. This means that our overlap integral factors into a two dimensional integral over Q_1 and Q_2 times a one dimensional integral over Q_3. Botter and Rosenstock[42] have shown that the matrix $\underline{\underline{J}}$ and the vector $\underline{K}$ can be expressed as

$$\underline{\underline{J}} = \underline{\underline{L}}'^{-1}\,\underline{\underline{Z}}\,\underline{\underline{L}} \quad \text{and}$$

$$\underline{K} = \underline{\underline{L}}'^{-1}\,\underline{R}$$

where $\underline{\underline{Z}}$ and $\underline{R}$ are functions only of the geometries of the molecule in the primed and the unprimed states and $\underline{\underline{L}}$ and $\underline{\underline{L}}'$ are the standard L matrices of normal mode analysis that connect symmetry and normal coordinates.[43] Botter and Rosenstock[42] explicitly present $\underline{\underline{Z}}$ and $\underline{R}$ for the case of C_{2v} symmetry.

This, plus standard normal mode analysis,[43] is all we require to calculate the overlap integrals $F(v_1',0,0 \leftarrow 0,0,0)$ under the harmonic oscillator approximation. We assume that the stretching force constant of O_3^- is 3.8 mdyne/Å and that the harmonic frequencies of O_3^- are $\omega_1 = 1010\ cm^{-1}$, $\omega_2 = 600\ cm^{-1}$, $\omega_3 = 800\ cm^{-1}$.[17,44] These values are only approximations of the harmonic frequencies since we have measured the fundamental frequencies ν_1 and ν_2 but have no information on the anharmonic constants; ω_3 is taken from the matrix work. This does not in fact much matter since, as in one dimensional Franck-Condon analysis, the overlap integrals are only weakly influenced by force constants and strongly by geometry differences (here $\underline{\underline{J}}$ is not very important, but $\underline{K}$ is and $\underline{K}$ is only a function of neutral O_3 normal mode analysis and the geometries of O_3 and O_3^-). For O_3[29,30] we take $r_e = 1.2717$ Å, α_e = bond angle = 116.78°, stretching force constant = 6.163 mdyne/Å, stretch-stretch interaction constant = 1.602 mdyne/Å, angle bending force constant = 2.102 mdyne/Å, and bend-stretch interaction constant = 0.511 mdyne. In the O_3^- calculation the last three force constants are determined by the three assumed harmonic frequencies.

The two dimensional Franck-Condon integrals are calculated numerically for various possible choices of the bond angle and bond distance for O_3^-. The experimental data to be fit are

$$[F(100 \leftarrow 000)/F_o]^2 = 1.45 \quad (10)$$

$$[F(200 \leftarrow 000)/F_o]^2 = 1.84 \quad (10)$$

$$[F(300 \leftarrow 000)/F_o]^2 = 1.32 \quad (10)$$

$$F_o \equiv F(000 \leftarrow 000)$$

where the peak heights were obtained from Fig. 2 by fitting the spectra with gaussian peak shapes. Unfortunately it turns out that given the experimental uncertainty in the peak heights and the uncertainty in the input to the normal mode analysis of O_3^- we cannot pinpoint an r_e, α_e for O_3^-, but rather we can find a locus of r_e, α_e points that does a reasonable job of fitting the data. These points range smoothly between (r_e = 1.36 Å, α_e = 118°), (r_e = 1.38 Å, α_e = 116½°), (r_e = 1.40 Å, α_e = 115°), (r_e = 1.42 Å, α_e = 114°) and extend somewhat on either side of this line. It is expected from molecular orbital arguments that the bond length of O_3^- is greater than that of O_3 (1.27 Å) and the bond angle is less than that of O_3 (117°). Cederbaum et al.[33] calculate that the bond length of O_3 increases by 0.10 Å and the angle decreases by 3.6° upon electron attachment. The matrix data gives the bond angle of O_3^- to be 108 ± 5°[15] and 110 ± 5°.[44] Andrews and Spiker[17] estimate the O_3^- bond length to be 1.38 ± 0.04 Å by comparing the stretching force constant of O_3^- from their matrix work to the bond lengths and force constants for O_2^- and O_2^{2-}. We find a relationship between allowed r_e and α_e dictated by the Franck-Condon analysis which is approximately α_e = (210.5 degrees - 68. degrees/Å × r_e) ± 1°.

C. Photodissociation of O_3^-

Experimentally we find that first ν_2 photodetachment transitions are suppressed by a factor of 20-100 for 2_0^n processes and by a factor of 3-20 for 2_n^0 processes, compared to analogous ν_1 transitions. Second, photodissociation dominates detachment.

The photodissociation data suggest that the "missing" intensity in the photodetachment cross section appears as threshold features in photodissociation. This observation leads us to imagine that ν_2 of an intermediate state is either along the dissociating coordinate or promotes to a dissociating state.

The valence configuration of O_3^- in C_{2v} symmetry can be represented by[45] $(3a_1)^2(2b_2)^2(4a_1)^2(5a_1)^2(1b_1)^2(3b_2)^2(4b_2)^2(6a_1)^2(1a_2)^2(2b_1)^1$, where a_1, a_2, b_1 and b_2 are the standard irreducible representations of C_{2v} and the coefficient orders the occurrence of orbitals of the same symmetry. The ground state as written above has overall electronic symmetry of $^2B_1$.

The two lowest excited electronic state which may be involved in the photodissociation process both involve electron promotion into the half filled $2b_1$ orbital:

$$O_3^-\ ^2B_1 + h\nu \rightarrow \begin{cases} O_3^-\ ^2A_2 \cdots (4b_2)^2(6a_1)^2(1a_2)^1(2b_1)^2 \\ \text{or} \\ O_3^-\ ^2A_1 \cdots (4b_2)^2(6a_1)^1(1a_2)^2(2b_1)^2 \end{cases} .$$

Cosby et al.,[5] in their study of O_3^- photodissociation, assign the dissociating state to be one of the above states. As Zare and coworkers have pointed out in a discussion of ClO_2,[46] which is isoelectronic with

O_3^-, putting electron density in the $2b_1$ orbital simultaneously promotes bending of the terminal oxygens and weakens bondings to the central atom. This is due to nodes between the central atom and terminal oxygens but no node between terminal oxygens in the $2b_1$ orbital. This suggests that ν_2 bending leading to formation of $O_2(^3\Sigma_g^-)$ from the terminal oxygen of O_3^- and $O^-(^2P)$ from the central oxygen might be a reasonable model for O_3^- photodissociation.

If dissociation indeed occurs by elimination of the central O^-, forming O_2 by joining together the two terminal O atoms, we may be specific about the electronic symmetry of the states involved. As noted above, we expect the dissociating state to be either $^2A_2$ or $^2A_1$. The products are O^- (^2P) and O_2 ($^3\Sigma_g^-$). If the dissociation occurs in the manner suggested, overall C_{2v} symmetry is retained, and we can examine the possible product symmetries in this group. In this way we can determine which of the states of O_3^- can dissociate to $O^- + O_2$. The O^- anion has either $^2A_1$, $^2B_1$, or $^2B_2$ symmetry, while the O_2 molecule has $^3A_2$ symmetry (the molecule is oriented with the C_2 axis passing perpendicularly through the diatomic molecular axis). Thus only three overall doublet symmetries can results from this dissociation: $^2A_2$, $^2B_2$, and $^2B_1$. This excludes the choice of a $^2A_1$ state as the precursor of these products, and the only likely state for dissociation is the $^2A_2$.

An interesting consequence of the above model and demanding conservation of orbital symmetry is that a cyclic ozonide species, however transient, must exist along the dissociation path. This arises from O_3^- having eight electrons of a_1 symmetry and six electrons of b_2 symmetry in its valance shell while the combination of $O_2(^3\Sigma_g^-) + O^-(^2P)$ has a total of ten electrons

of a_1 and four electrons of b_2 symmetry in the valence shell. In D_{3h} symmetry, that of cyclic ozonide, a_1 and b_2 orbitals can become degenerate and mix, allowing the photodissociation fragments to leave with the proper number of electrons of each symmetry.

Zare and coworkers likewise predict central atom attack by incoming alkaline earth metals on excited $C\ell O_2$.[46] They picture an electron jump from the metal atom to $C\ell O_2$ that fills the $2b_1$ orbital, facilitating the attack of the central $C\ell$ by the incoming metal cation. We note that Jacox and Milligan,[44] in somewhat the reverse experiment, produced O_3^- in an argon/O_2 matrix with a source of $^{18}O^-$ from enriched $N_2{}^{18}O$ + metal + uv light. They found substantial amounts of $O^{16}O^{18}O^{16-}$, but interpreted this as end-on attack of $^{18}O^- + {}^{16}O_2$ followed by photodissociation, scrambling, and recombination. Recent results of Meisels and coworkers[47] on photoionization of SO_2 shows that bending quanta transitions which should result in excitation of SO_2^+ instead produce S^+.

While the model presented to explain O_3^- photodissociation fits nicely into a consistent pattern, it may be that ν_2 vibrations promote dissociation along the asymmetric coordinate. The 2_n^0 photodetachment transitions are unexpectedly weak for this model and not all 2_n^m $n,m > 0$ transitions have been found in the photodissociation spectrum. In addition, the symmetry labels of the electronic orbitals are not rigorous and the exact dynamics of the photodetachment/photodissociation process are not well understood; therefore the process $O_3^- + h\nu \rightarrow O_2 + O^-$ need not conserve orbital geometry. It is possible that ν_2 then only provides either a coupling or a facile geometry for dissociation in the asymmetric coordinate.

Neither model, as presented so far, explains why neutral $O_3(\nu_2)$ quantum numbers and frequencies should provide a convincing description of O_3^- photodissociation, or why photodissociation dominates photodetachment. Although the exact description lies buried in the quantum description of the photodetachment/photodissociation process, a starting point is to consider that upon absorption of a photon, O_3^- is excited to a complex state $O_3^-\ {}^2B_1 + h\nu \rightarrow (O_3 + e)^2A_2$. The complex can be viewed as arising from the ability of the electron to make large excursions from the nuclei before the nuclei react to the absorption of the photon. For example, consider the situation where the photodissociation and the photodetachment channels are both closed and for the case of photodetachment the energy is only slightly below threshold. The electron can then make a large excursion from the nuclear frame before its kinetic energy is overcome by the attractive potential of the system. (See Rau and Fano[48] and references therein for complex formation in the case of photodetachment from atoms.) The further the electron is removed from the core O_3, the more closely the vibrational frequencies should resemble O_3 rather than O_3^{-*}.

Given the difficulties in determining the detailed dynamics of a complex system the best that can be said about the photodetachment/photodissociation process in O_3^- is the following. O_3^- absorbs a photon

$$O_3^-(^2B_1) + h\nu \rightarrow (O_3 + e^-)$$

to a complex of $^2A_2$ symmetry. There are two competing channels for the O_3^- complex, detachment and dissociation

$$O_3^-(^2A_2) \rightarrow \begin{cases} O_3(^1A_1) + e^- \\ O_2(^3\Sigma_g^-) + O^-(^2P) \end{cases} .$$

Dissociation is fast compared with photodetachment and might either proceed or be aided by motion, other than zero pt, in the bending coordinate of the neutral-like species.

D. Excited electronic states

In the previous section we invoked the existence of a $^2A_2$ excited electronic state of O_3^- to explain the dissociation of the ion into $O_2 + O^-$. This state was implicitly assumed to be very short lived on the time scale of our experiment. Long lived excited states of the ozonide ion, which for us means $\tau > 5$ μsec, would appear as peaks of high electron kinetic energy in the photoelectron spectrum. We see no evidence for such a state. Cosby et al.[5] in their study of the photodissociation of O_3^- assign features in their spectra to the state we would assign as $^2A_2$. Tiernan and coworkers find evidence for vibrational excitation of the ozonide ion.[4] In their experiment, different thresholds were observed for the collision induced dissociation of O_3^- depending on the mode of production of the ion. Their ion flight time implies lifetimes on the order of several microseconds or greater. The greatest excitation was produced by electron impact on mixtures of O_3 and N_2O, whereas the ground state was formed using mixtures of O_3 and H_2O. N_2O is here primarily a source of O^- and thus our preparation of O_3^- from "neat" ozone is most closely analogous to Tiernan's excited state production scheme. The reason for the different degrees of excitation is not at all obvious. If we had produced substantial populations of an excited state of O_3^- with a lifetime of 10 μsec we probably would have observed it in the photoelectron experiment, since approximately 30 μsec elapse between ion formation and interaction with the laser beam.

The excited state of neutral ozone that we find in the UV photoelectron spectrum is perhaps 0.7 to 1.1 eV (6000-9000 cm^{-1}) above the ground state. While we can make no assignment of the few indistinct peaks observed, it appears that the peaks associated with detachment to this state are more closely packed than can be explained by a progression in the symmetric stretch alone. It is likely that here a ν_2 progression is responsible for the "extra" peaks.

The calculations on the D_{3h} state of neutral ozone at the present time put the state at quite different energies. Burton and Harvey[21] predict it to be 0.2 eV above the ground state, Hay et al.[22,23] at least 1.4 eV above, Wright[24] 2 eV below, and Shih et al.[49] 0.65 eV above the ground state. There are other C_{2v} excited states of O_3 that are also possible candidates including a low-lying (1.0-1.4 eV) $^3B_2$,[22,50] which is not optically accessible from the $^1A_1$ ground state.

V. SUMMARY

We have measured the electron affinity of ozone $EA(O_3) = 2.1028(25)$ eV, and the symmetric stretching and bending frequencies of the ozonide ion to be 982(30) cm^{-1} and 550(50) cm^{-1}, respectively. Two dimensional harmonic Franck-Condon analysis gives the bond length of the negative ion to be greater and the angle to be slightly less than that of the neutral. While no evidence was found for a long lived excited electronic state of the ozonide ion, a new excited electronic state of neutral ozone is revealed perhaps 0.7 to 1.1 eV above the ground state. The lack of a strong bending mode in detachment suggests a dissociating mechanism whereby O_3^- dissociates to $O_2 + O^-$ via the bending coordinate. Attempts to measure the electron affinity of CO_3^- were unsuccessful.

VI. ACKNOWLEDGMENTS

It is with profound sadness that we dedicate this paper to Professor Herbert P. Broida whose untimely death has deprived the scientific community of a dynamic and diverse investigator, and the authors of a valued friend and summer colleague.

Fred Fehsenfeld and Eldon Ferguson were very helpful in discussing their experiments with us and pointing out the importance of the electron affinity measurement. We would like to thank Peter Burton for interesting discussions on his work on symmetric ozone, and Carl Howard and George Lawrence who made ozonizers available to us. WCL is pleased to acknowledge the hospitality of the Aspen Center for Physics during a portion of the preparation of this manuscript. This work was supported in part by Army Research Office grant DAAG29-76-G-0236, and in part by National Science Foundation grants PHY76-04761 and CHE75-01565 through the University of Colorado.

REFERENCES

*Present address: Department of Chemistry, Wesleyan University, Middletown, CT 06457.

†Present address: Department of Chemistry, University of Oregon, Eugene, OR 97403.

‡JILA Visiting Fellow; permanent address: Department of Chemistry, University of Utah, Salt Lake City, UT 84112.

§Camille and Henry Dreyfus Teacher-Scholar.

1. J. R. Peterson, J. Geophys. Res. 81, 1433 (1976).

2. I. Dotan, J. A. Davidson, G. E. Streit, D. L. Albritton, and F. C. Fehsenfeld, J. Chem. Phys. 67, 2874 (1977).

3. C. Lifshitz, R. L. C. Wu, T. O. Tiernan and D. T. Terwilliger, J. Chem. Phys. 68, 247 (1978).

4. R. L. C. Wu, T. O. Tiernan and C. Lifshitz, Chem. Phys. Lett. 51, 211 (1977).

5. P. C. Cosby, J. T. Moseley, J. R. Peterson and J. H. Ling, J. Chem. Phys. 69, 2771 (1978).

6. P. C. Cosby, R. A. Bennett, J. R. Peterson and J. T. Moseley, J. Chem. Phys. 63, 1612 (1975).

7. M. L. Vestal and G. H. Mauclaire, J. Chem. Phys. 67, 3767 (1977).

8. N. Swanson and R. J. Celotta, Phys. Rev. Lett. 35, 783 (1975).

9. S. F. Wong, T. V. Vorburger and S. B. Woo, Phys. Rev. A 5, 2598 (1972).

10. R. Byerly Jr. and E. C. Beaty, J. Geophys. Res. 76, 4596 (1971).

11. a) M. W. Siegel, R. J. Celotta, J. L. Hall, J. Levine and R. A. Bennett, Phys. Rev. A 6, 607 (1972); b) R. J. Celotta, R. A. Bennett and J. L. Hall, J. Chem. Phys. 60, 1740 (1974); c) R. J. Celotta, R. A. Bennett, J. L. Hall, M. W. Siegel and J. Levine, Phys. Rev. A 6, 631 (1972).

12. H. Hotop, R. A. Bennett and W. C. Lineberger, J. Chem. Phys. 58, 2373 (1973); H. Hotop and W. C. Lineberger, J. Phys. Chem. Ref. Data 4, 539 (1975).

13. B. Rosen, Spectroscopic Data Relative to Diatomic Molecules, Vol. 17 of International Tables of Selective Constants (Pergamon Press 1970).

14. a) J. Slater, F. H. Read, S. E. Novick and W. C. Lineberger, Phys. Rev. A 17, 201 (1978), for the latest modifications; b) H. Hotop, T. A. Patterson, and W. C. Lineberger, Phys. Rev. A 8, 762 (1973) for the basic design.

15. A. Barbe, C. Secroun and P. Jouve, J. Mol. Spectrosc. 49, 171 (1974).

16. S. A. Clough and F. X. Kneizys, J. Chem. Phys. 44, 1855 (1966).

17. L. Andrews and R. C. Spiker, J. Chem. Phys. 59, 1863 (1973).

18. J. B. Bates, Chem. Phys. Lett. 26, 75 (1974).

19. J. B. Bates and J. C. Pigg, J. Chem. Phys. 62, 4227 (1975).

20. G. Herzberg, Molecular Spectra and Molecular Structure III. Polyatomic Molecules (Van Nostrand, 1966).

21. P. G. Burton and M. D. Harvey, Nature 266, 826 (1977); P. G. Burton, private communication.

22. P. J. Hay, T. H. Dunning and W. A. Goddard III, J. Chem. Phys. 62, 3912 (1975).

23. P. J. Hay and W. A. Goddard III, Chem. Phys. Lett. 14, 46 (1972).

24. J. S. Wright, Can. J. Chem. 51, 140 (1973).

25. L. M. Branscomb, S. J. Smith, G. Tisone, J. Chem. Phys. 43, 2906 (1965).

26. S. P. Hong, S. B. Woo, E. M. Helmy, Phys. Rev. A 15, 1563 (1977).

27. E. P. Wigner, Phys. Rev. 73, 1002 (1948).

28. K. J. Reed, A. H. Zimmerman, H. C. Andersen and J. I. Brauman, J. Chem. Phys. 64, 1368 (1976).

29. P. L. Jones, S. E. Novick, J. H. Futrell and W. C. Lineberger, to be published.

30. K. M. Mack and J. S. Muenter, J. Chem. Phys. 66, 5278 (1977).

31. R. Trambarulo, S. N. Ghosh, C. A. Burrus Jr. and W. Gordy, J. Chem. Phys. 21, 851 (1953).

32. T. Tanka and Y. Morino, J. Mol. Spectrosc. 33, 552 (1970).

33. L. S. Cederbaum, W. Domcke and W. von Niessen, Mol. Phys. 33, 1399 (1977).

34. E. W. Rothe, S. Y. Tang and G. P. Reck, J. Chem. Phys. 62, 3829 (1975).

35. R. H. Wood and L. A. D'Orazio, J. Phys. Chem. 69, 2562 (1965).

36. M. M. Heaton, A. Pipano, J. J. Kaufman, Int. J. Quant. Chem. Symp. 6, 181 (1972).

37. J. Berkowitz, W. A. Chupka and D. Gutman, J. Chem. Phys. 55, 2733 (1971).

38. J. T. Moseley, P. C. Cosby and J. R. Peterson, J. Chem. Phys. 65, 2512 (1976).

39. S. W. Benson, Thermochemical Kinetics (Wiley, New York, 1976), 2nd ed.

40. J. L. Gole and R. N. Zare, J. Chem. Phys. 57, 5331 (1972).

41. F. Duschinsky, Acta Physicochim. URSS 7, 551 (1937).

42. R. Botter and H. M. Rosenstock, J. Res. Nat. Bur. Stand. Sect. A 73, 313 (1969).

43. E. B. Wilson, Jr., J. C. Decius and P. C. Cross, Molecular Vibrations (McGraw-Hill, New York, 1955).

44 M. F. Jacox and D. E. Milligan, J. Mol. Spectrosc. 43, 148 (1972).

45. W. L. Jorgensen and L. Salem, The Organic Chemists Book of Orbitals (Academic Press, New York, 1973).

46. F. Engelke, R. K. Sander and R. N. Zare, J. Chem. Phys. 65, 1146 (1976).

47. G. C. Meisels, private communication.

48. A. R. P. Rau and U. Fano, Phys. Rev. A 4, 1751 (1971).

49. S. Shih, R. J. Buekner and S. D. Peyerimhoff, Chem. Phys. Lett. 28, 463 (1974).

50. K.-H. Thunemann, S. D. Peyerimhoff and R. J. Buenker, J. Mol. Spectrosc. 70, 432 (1978).

51. R. C. Spiker, Jr. and L. Andrews, J. Chem. Phys. 49, 1851 (1973).

52. R. L. C. Wu and T. O. Tiernan, 31st Annual Gaseous Electronics Conference Bull. Am. Phys. Soc. (in press).

Table 1. Spectroscopic assignments from the tunable laser experiments

Frequency ± 10 cm^{-1} [a]	Assignment	Derived Constant [b] (cm^{-1})	Channel [e]
15978(20)	1_1^0	$\nu_1'' = 982(30)$ [c]	DET
16415(30)	2_1^0	$\nu_2'' = 550(50)$ [c]	DET
16960(20)	0-0	$EA(O_3) = 16960(20)$ [c]	DET
17076(30)	1_1^1	$\nu_1'' = 990(40)$ [d]	DET
17206(30)	1_2^2	$\nu_1'' = 980(40)$ [d]	DET
17681(30)	2_0^1	$\nu_2' = 720(40)$	DES/DET
18057(20)	1_0^1	$\nu_1' = 1100(30)$	DET

[a] This 10 cm^{-1} is a rotational correction (see text)

[b] Double primes refer to O_3; single prime to O_3

[c] Our recommended value

[d] $\nu_1' = 1103$ cm^{-1} used in deriving this result

[e] DET is photodetachment; DES is photodestruction

Table II. Vibrational frequencies of O_3 and O_3^-

Vibrational Frequency	Reference
Symmetric stretch of neutral ozone (cm^{-1})	
1100(30)	photodetachment (present study)
1090(30)	photoelectron (present study)
1103.15	15,16 infrared spectra
Symmetric bend of neutral ozone (cm^{-1})	
720(40)	photodestruction & photodetachment (present study)
700.96	15,32 infrared spectra
Symmetric stretch of the ozonide ion (cm^{-1})	
982(30)[a]	photodetachment (present study)
1040(60)	photoelectron (present study)
790(50) or 928(50)	5; photodissociation
1012-1026	17; matrix Raman spectra
1012-1032	18,19; single crystal Raman spectra
Symmetric bend of the ozonide ion (cm^{-1})	
550(50)[a]	photodestruction (present study)
419(20) or 403(20)	5; photodissociation
587-619	51; matrix infrared spectra

[a]Recommended values

Table III. Electron affinity of ozone

Electron Affinity (eV)	Reference
2.1028(25)[a]	photodetachment (present study)
2.103(20)	photoelectron (present study)
1.99(10)	9; photodetachment
≥1.82	2; ("true" lower limit) reactive thermochemical equilibria in a flowing afterglow
$\geq 2.26\ ^{+0.04}_{-0.06}$	3; (lower limit) endothermic charge transfer
2.1(1)	10; photodetachment
2.14(15)	34; collisional ionization
≥1.96	37; (lower limit) endothermic charge transfer
1.9(4)	35; lattice energy
2.12	36; C.I. calculation vertical electron affinity
2.2(1)	4; translational energy threshold for bond dissociation

[a]Our recommended value

FIGURE CAPTIONS

Fig. 1. Photoelectron spectrum of O_3^-. The photon energy is 2.540 eV (488 nm). The peak labeled 0-0 is the vibrational origin, and the vibrational notation is defined in the text. The large peak at 1.07 eV is due to O^- detachment, the O^- being produced by photodissociation of O_3^-.

Fig. 2. Photoelectron spectrum of O_3^-. The photon energy is 3.407 eV (363.8 nm). The progression from Fig. 1 is further developed. There are also a series of vibrationally unassigned peaks at low electron kinetic energy that are due to a new electronic state of neutral ozone.

Fig. 3. Photodestruction (upper curve) and photodetachment spectrum (lower curve) of O_3^-. The relative scales of the two cross sections are obtained from the absolute count rates of neutrals and electrons and from an estimation for the relative efficiencies of the two detectors and should be taken as an approximation only. The vibrational notation is defined in the text. The features 1_1^0, 0-0, 1_1^1, 1_2^2, 2_0^1 and 1_0^1 are assigned from the photodetachment cross section; 2_0^2 is placed at the position expected on the basis of known frequencies.

Fig. 4. High resolution photodetachment cross section in the region of the vibrational origin (Electron Affinity of ozone). The laser linewidth is 1.3 cm^{-1}.

Fig. 5. Low resolution photodestruction (upper curve) and photodetachment cross sections. The electron extraction field is set low so as to detect only very low energy electrons. This allows us to bring out the weak feature 2_1^0 in the photodetachment curve not seen in Fig. 3.

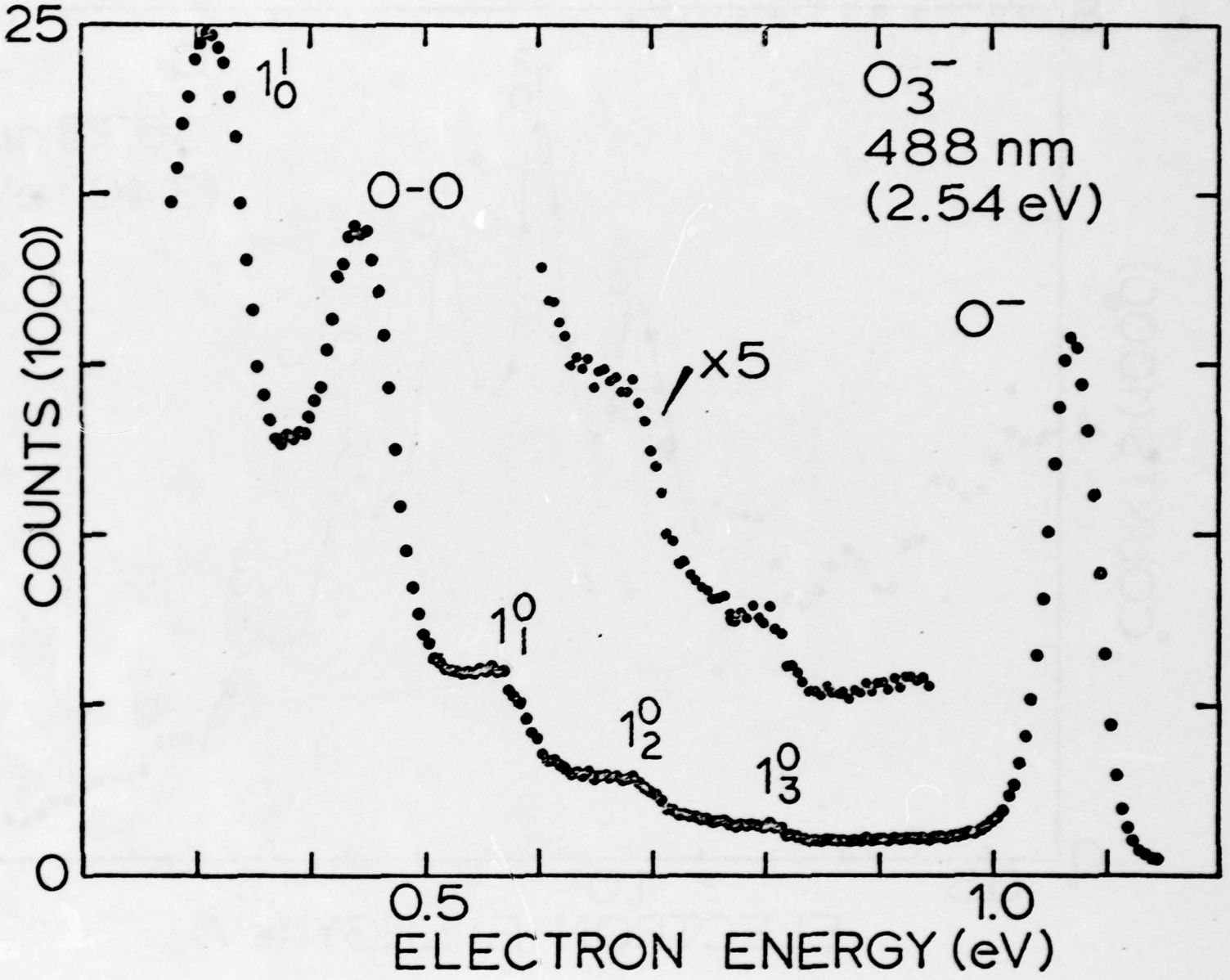
25
0
COUNTS (1000)
1_0^1
0-0
O_3^-
488 nm
(2.54 eV)
O^-
x5
1_1^0
1_2^0
1_3^0
0.5
1.0
ELECTRON ENERGY (eV)

Figure 1

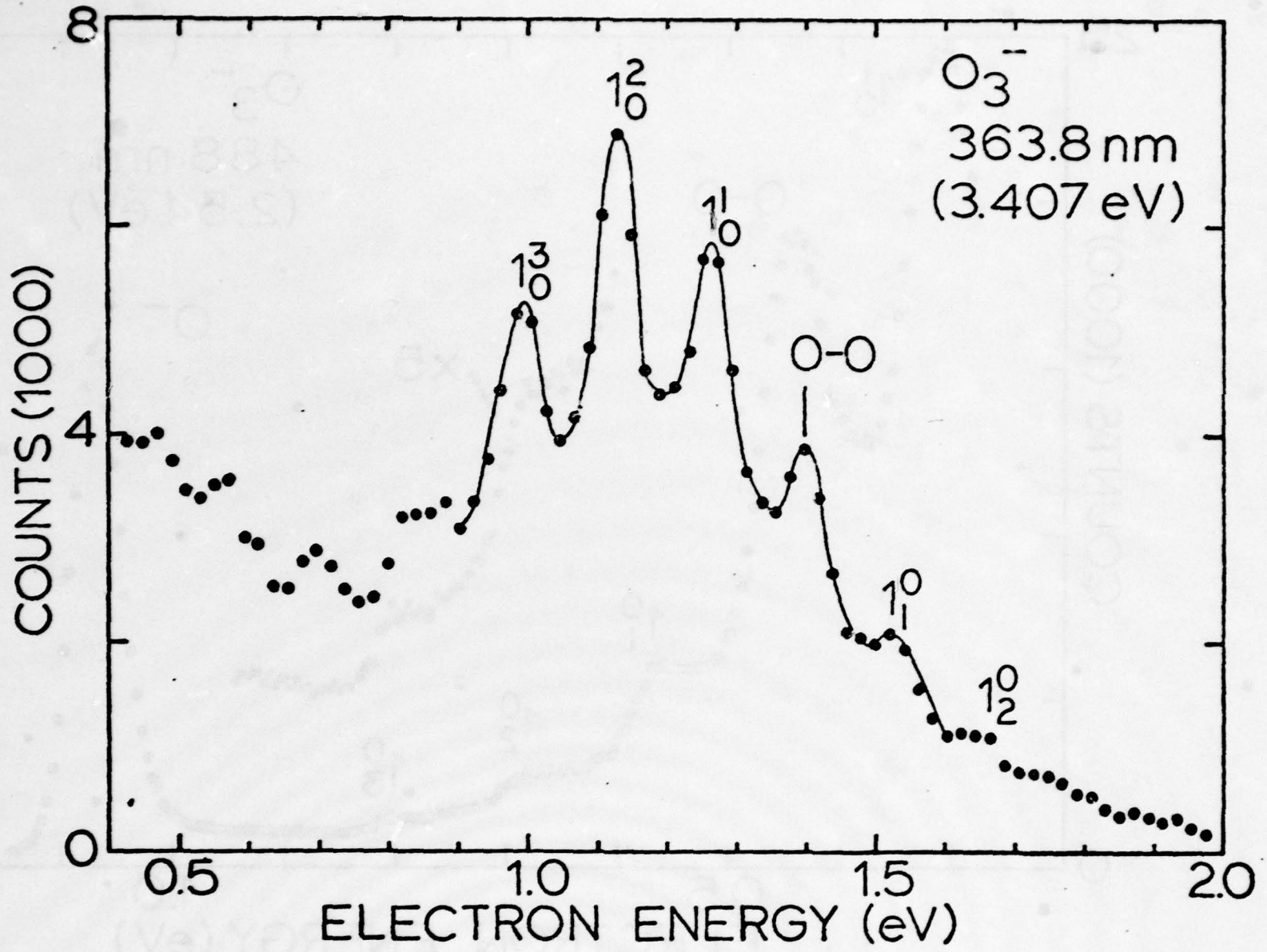
8
4
0
COUNTS (1000)
0.5
1.0
1.5
2.0
ELECTRON ENERGY (eV)
O_3^-
363.8 nm
(3.407 eV)
1_0^2
1_0^3
1_0^1
0-0
1_1^0
1_2^0

Figure 2

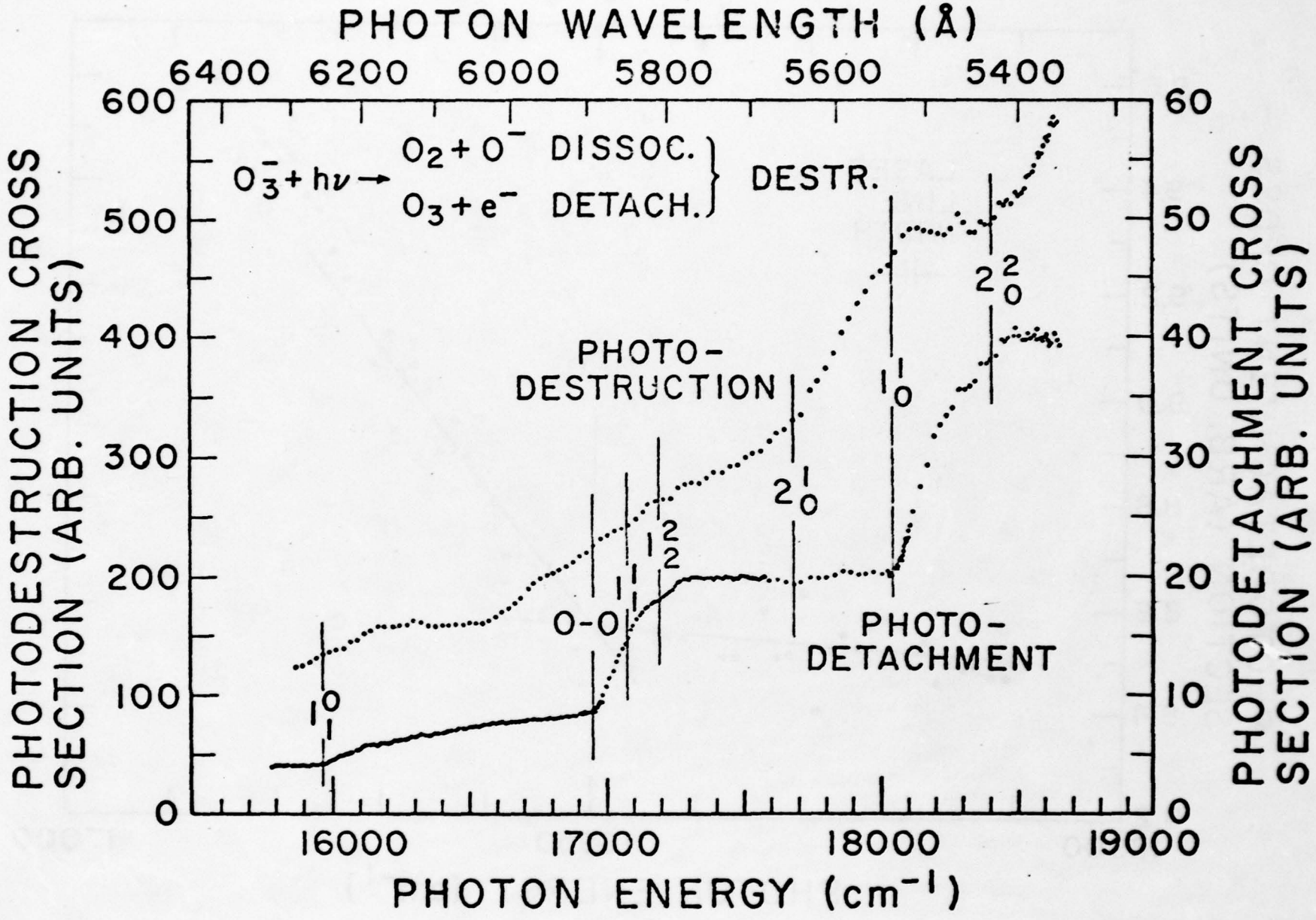
PHOTON WAVELENGTH (Å)
6400 6200 6000 5800 5600 5400
600 500 400 300 200 100 0
60 50 40 30 20 10 0
PHOTODESTRUCTION CROSS SECTION (ARB. UNITS)
PHOTODETACHMENT CROSS SECTION (ARB. UNITS)
$O_3^- + h\nu \rightarrow$ $O_2 + O^-$ DISSOC. $O_3 + e^-$ DETACH. } DESTR.
PHOTO-DESTRUCTION
PHOTO-DETACHMENT
0-0
1 0
2 0
1 1
2 1
1 2
2 2
16000 17000 18000 19000
PHOTON ENERGY (cm^{-1})

Figure 3

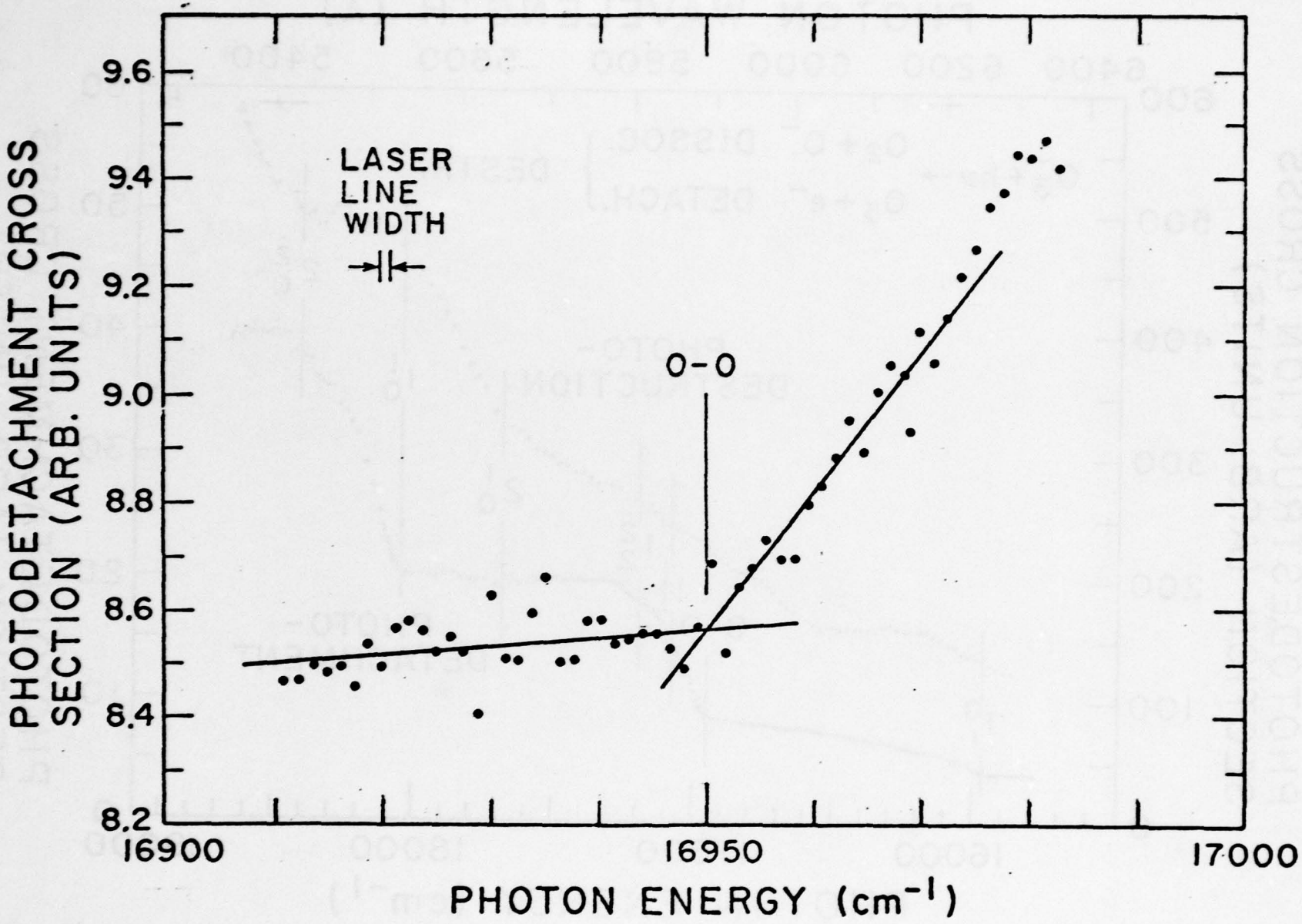
PHOTODETACHMENT CROSS SECTION (ARB. UNITS)
9.6
9.4
9.2
9.0
8.8
8.6
8.4
8.2
LASER LINE WIDTH
0-0
16900
16950
17000
PHOTON ENERGY (cm⁻¹)

Figure 4

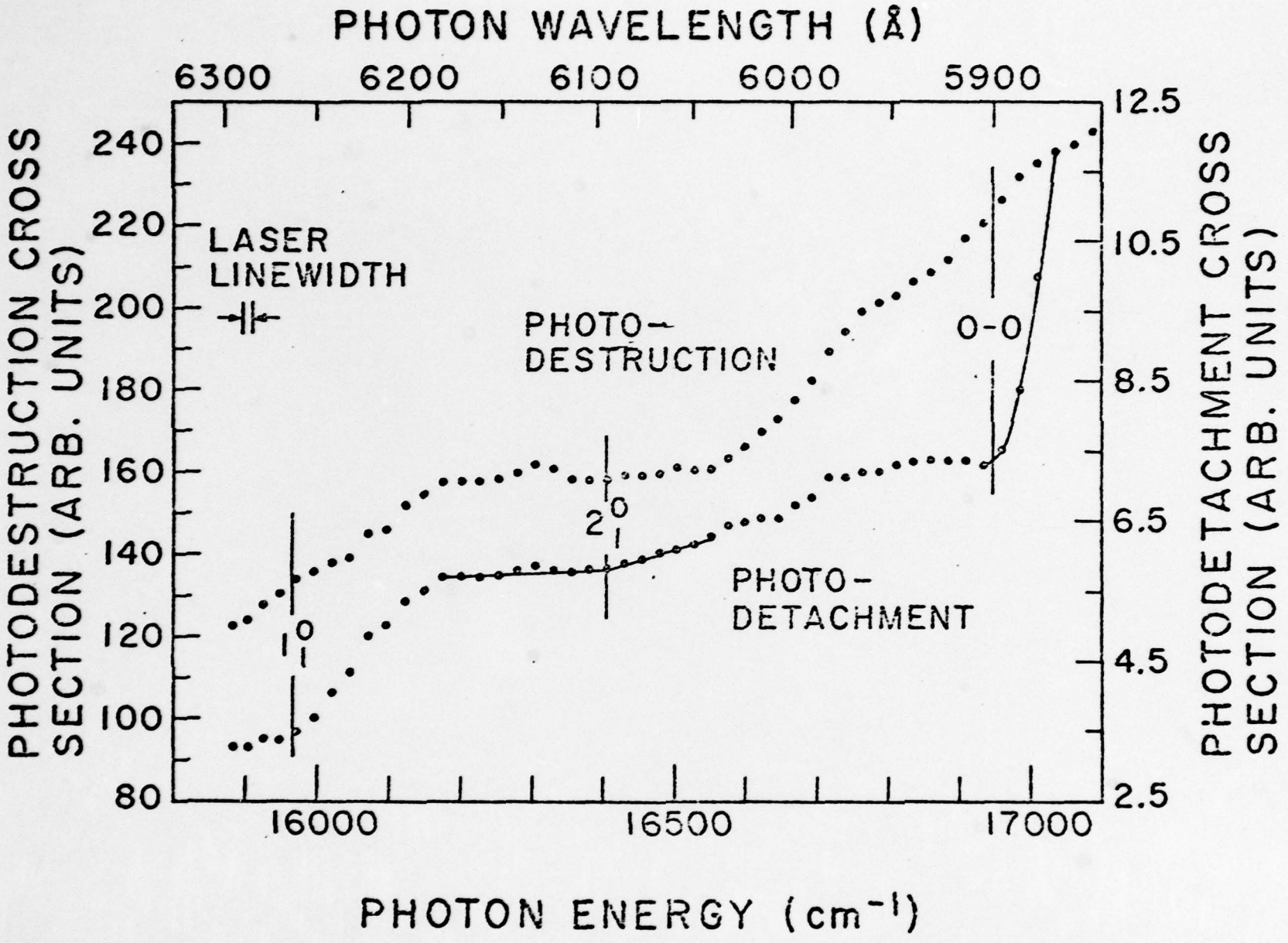
PHOTON WAVELENGTH (Å)
6300
6200
6100
6000
5900
PHOTODESTRUCTION CROSS SECTION (ARB. UNITS)
240
220
200
180
160
140
120
100
80
LASER LINEWIDTH
PHOTO-DESTRUCTION
0-0
2 0
1 0
PHOTO-DETACHMENT
12.5
10.5
8.5
6.5
4.5
2.5
PHOTODETACHMENT CROSS SECTION (ARB. UNITS)
16000
16500
17000
PHOTON ENERGY (cm⁻¹)

Figure 5